

Article

# Remote Detection of Growth Dynamics in Red Lettuce Using a Novel Chlorophyll *a* Fluorometer

Matthew R. Urschel and Tessa Pocock \*

Center for Lighting Enabled Systems and Applications (LESA), Rensselaer Polytechnic Institute (RPI), Troy, NY 12180, USA; urschm@rpi.edu

\* Correspondence: pocock@rpi.edu; Tel.: +1-518-276-7220

Received: 22 August 2018; Accepted: 11 October 2018; Published: 16 October 2018



**Abstract:** The production of food crops in controlled environment agriculture (CEA) can help mitigate food insecurity that may result from increasingly frequent and severe weather events in agricultural areas. Lighting is an absolute requirement for crop growth in CEA, and is undergoing rapid advances with the advent of tunable, light emitting diode (LED) systems. The integration of these systems into existing CEA environmental control architectures is in its infancy and would benefit from a non-invasive, rapid, real-time, remote sensor that could track crop growth under different lighting regimes. A newly-developed remote chlorophyll *a* fluorescence (ChlF) sensing device is described herein that provides direct, remote, real-time physiological data collection for integration into tunable LED lighting control systems, thereby enabling better control of crop growth and energy efficiency. Data collected by this device can be used to accurately model growth of red lettuce plants. In addition to monitoring growth, this system can predict relative growth rates (RGR), net assimilation rates (NAR), plant area (PA), and leaf area ratio (LAR).

**Keywords:** chlorophyll fluorescence; controlled environment agriculture; crop growth; crop modeling; relative growth rates; remote sensing; light emitting diodes

## 1. Introduction

Evidence for anthropogenic climate change along with predicted demographic trends toward increased habitation in cities are imposing new challenges on global agriculture and are threatening food security for a global population that is projected to reach 11.2 billion people by the end of the 21st century [1,2]. This, together with the growing demand for fresh, locally-grown produce and shifts toward plant-based diets has attracted renewed interest in controlled environment agriculture (CEA). CEA protects crops from inclement weather while allowing for consistent and predictable crop production through rigorous environmental control. CEA sensing and control systems have existed for over fifty years and typically involve the control of environmental parameters, such as light, temperature, CO<sub>2</sub>, and relative humidity. Real-time environmental data are used to modulate ventilation, heating, fog systems, shade systems, and supplemental lighting [3]. Electric lighting can account for up to 30% of the total energy cost, but needs to be optimized to make CEA more economically viable while also reducing its carbon footprint [4]. The daily light integral is the accumulated light reaching the canopy, and is measured as moles of photons m<sup>-2</sup> day<sup>-1</sup> within the photosynthetically-active radiation (PAR) region of 400–700 nm. It is specific for different crops and is positively correlated with growth and crop yield. Most light control systems are based on instantaneous light values, past weather, or predictive weather patterns, but systems based on the accumulation of PAR during the day (DLI) have resulted in further optimization of crop yield and energy use [5,6]. Use of supplemental and sole source (no sun) lighting technology is expanding in CEA as the importance of spectral variation on plant growth and physiological responses becomes apparent [7]. New methods

and models are needed to quantify crop growth remotely and non-invasively, better predict crop growth using different lighting technologies, assess the performance of new cultivars, and advance the state of the art in CEA through knowledge gained from fundamental research. Here, we used a newly-developed chlorophyll *a* fluorescence (ChlF) sensor to remotely monitor growth of red lettuce in real-time. Regression analysis was subsequently used to construct models from this data that accurately predicted observed growth rates based on measured ChlF values. The increases in ChlF were determined to be due to growth and not changes in leaf pigmentation, especially chlorophyll *a*, the source of ChlF.

The relative growth rate (RGR) of a plant is defined as the rate of mass increase per unit mass present, and provides a measure of the efficiency of plant growth normalized to total biomass. Evaluating the RGR allows for the equitable comparison of growth rates between different plant species or individuals by accounting for variations in scale between them [8]. In addition, the RGR has been demonstrated to be predictive of plant mortality and can indicate the nutritional status of plants [9,10]. Plant growth kinetic analyses can be fitted to a linear or exponential model and the RGR is then calculated as the slope of the natural logarithm-transformed mean fresh (FW) or dry (DW) weight [11,12]. Calculating RGR from direct physical measurements of plant FW or DW is laborious and destructive to plants. Therefore, a new, simple, and non-destructive method for collecting time series growth data remotely would greatly facilitate studies of growth kinetics. To this end, many techniques for remotely sensing plant growth have been investigated over the last several decades. Development of plant growth models based on image processing, machine vision and neural networks for photographic growth monitoring have been in use since the 1990s, but these methods have not been widely adopted (reviewed in [3]). Image sensing and processing has been used to predict crop harvest dates for lettuce and time to first flower for tomatoes, however, this method involves heavy computation and is sensitive to ambient light or changes in other environmental parameters [3,10]. The use of remotely-sensed chlorophyll *a* fluorescence (ChlF) as a proxy for plant growth kinetics in real-time has also been explored. Although typically used in satellite imaging, several different ChlF platforms have been described that can be used to measure growth or photosynthetic performance in CEA settings.

Chlorophyll fluorescence is a natural process whereby light energy absorbed by chlorophyll *a* molecules is re-emitted as light in the red and far-red regions. The ChlF emission spectrum at room temperature ranges from approximately 650 nm to 780 nm with distinct peak maxima at 685 nm and between 720–740 nm [13]. The measurement of ChlF is non-invasive and rapid, and this powerful technique has been used for decades as a probe for photosynthetic activity, to detect stress and to understand photosynthetic regulation of biochemical pathways and gene expression [14–16]. Functionally, ChlF yields are inversely proportional to photosynthetic rates [14]. ChlF is also a useful tool to test agricultural productivity, physiological status of newly bred cultivars, the health of fresh produce, and in optimizing plant growth conditions (i.e., temperature, light, etc.) for economic optimization of crop plants in CEA [15]. There are many accepted ChlF methodologies based on different instruments and timescales of data capture, but they require direct contact or close proximity to the leaf (<2.0 cm) (reviewed in [13]). ChlF fluorometers consist of two main components, the first involves active (lamps, lasers) or passive (solar) light-induced excitation of chlorophyll *a* molecules, while the second component measures the resulting ChlF using optical fibers, satellite images, or photodiodes [17,18]. Spectroradiometers employing optical fiber systems have been used for direct ChlF measurements and these measurements have been shown to correlate with growth and photosynthetic efficiency [19,20]. A relationship has also been observed between dry weight accumulation and spectrally sensed red (665–675 nm) to far-red (740–750 nm) ratios in basil crops, suggesting this ratio may also be useful for monitoring growth, however, the signal detected in the study is largely due to leaf reflectance [21]. Most commercial pulse amplitude modulated ChlF research systems used in stress physiology and ecophysiology use photodiodes as sensors; they are low cost, small, and have fast response times [16,17]. ChlF biofeedback systems that adjust PAR values

to plant physiology processes, for example, electron transport rates, have successfully been used to regulate and maintain photosynthetic rates but the close proximity to the leaf (~1.2 cm), the small field of view (~10 mm) and the saturating pulses were impractical and damaging to the plant [22]. The effective quantum yields decreased over time due to photoinhibition caused by frequent exposure to the saturating pulses of between 8000 and 12,000  $\mu\text{mol m}^{-2} \text{s}^{-1}$ . The above studies indicate that ChlF is a good candidate for the advancement of crop growth modeling, but improvements need to be made on the methodology, optics, and hardware.

Kinetic growth analyses provide insight into the rates of plant physiological processes underlying growth and allow plant growth outcomes to be predicted and adjusted. They are also a useful research tool for assessing the effects of different environments on plants or the performance of newly bred cultivars. During the last five years, a total of twelve undergraduate engineering students participated in a sensing project in the Lighting Enabled Systems and Applications (LESA) plant physiology laboratory at Rensselaer Polytechnic University (RPI) (NY). The goal was to come up with a low-cost ChlF detector that could work remotely (1–1.5 m from the canopy) with a reasonable field of view in order to accurately track plant growth under sole source lighting (no sun). Here we report growth kinetic analyses on the red lettuce cultivar Rouxai using the standard method of time series biomass collection and a model created from the newly-developed sensing system. Known as the Fluorescence Undergraduate Sensing SYstem (FUSSY), this system is an active (LED), room temperature, photodiode-based ChlF system. In addition to RGR, data from FUSSY also allowed us to confidently predict leaf area ratio (LAR) and net assimilation rate (NAR), both of which are predictive of crop growth processes [23,24]. This communication describes FUSSY, and outlines its potential use as a direct, physiological, real-time remote-sensing system for integration into tunable LED systems for better control of crop growth.

## 2. Materials and Methods

### 2.1. Plant Cultivation

The chlorophyll *a* fluorescence (ChlF) detection system (FUSSY) was used to monitor real-time growth dynamics of Red Oakleaf lettuce (*Lactuca sativa* cv. Rouxai) grown in controlled environment growth chambers (Conviron A1000, Winnipeg, MB, Canada). These experiments were aimed at quantifying the relationship between growth and measured ChlF and to demonstrate that ChlF data remotely collected by this device can serve as an accurate proxy for lettuce growth. Rouxai red lettuce seeds (Cat. No. 3061.11) were obtained from Johnny's Selected Seeds (Winslow, ME, USA). They were seeded in Grodan 1'' Rockwool AX plugs (Grodan, Roermond, The Netherlands) in standard 1020 flats with 6 × 13 inserts (Gro-Smart Tray-Terracotta Model HDR1035-1, Grodan, Roermond, The Netherlands) at a constant day/night temperature of 23 °C and relative humidity of 70%. Temperature, relative humidity and atmospheric CO<sub>2</sub> concentration were monitored by a Green Eye Desktop CO<sub>2</sub>, Temperature and Relative Humidity Monitor, (Model TIM-12, Global Sensors, Belmont, NC, USA) placed in the growth cabinet at canopy level. Plants were grown under 24 h photoperiods for 17 days at 200  $\mu\text{mol m}^{-2} \text{s}^{-1}$  PAR under cool white fluorescent (CWF) tubes (Philips, F32T8/TL841, 800 series, Amsterdam, The Netherlands) and watered with half strength Hoagland's solution [25].

### 2.2. Plant Growth Kinetics

Above ground fresh (FW) and dry (DW) weights and plant area (PA) were measured at intervals over a 17 day growth period. Three plants were sampled from random positions in the growth tray at 12 time points (5, 7, 9, 10, 11, 12, 13, 14, 15, 16, and 17 days after seeding (DAS)) (Figure A1). Fresh weights (g) of individual plants were measured immediately after harvest and digitally photographed on a well-lighted, flat surface next to a 2 cm<sup>2</sup> red scaling square to measure plant area (PA). The area of green pixels in each photograph was calculated using Easy Leaf Area plant area image analysis

software [26]. Individual plants were dried to constant weight in a drying oven at 70 °C. Plants were cooled prior to each weighing in a desiccator with calcium sulfate ( $\text{CaSO}_4$ ) desiccant (W.A. Hammond DRIERITE Co. LTD, Xenia, OH, USA) until they reached constant weight (approx. 72 h). Harvests were performed at the same time (2 h into the photoperiod) each day and were synchronized so that plants were always harvested immediately after a ChlF measurement.

### 2.3. Plant Pigment Analyses

An additional three plants were sampled at five of the 12 time points described above (9, 11, 13, 15, and 17 DAS) to measure chlorophyll, carotenoid, and anthocyanin concentrations.

Plants were flash frozen in liquid nitrogen ( $\text{N}_2$ ) and ground to a fine powder immediately after removal from the growth chamber. Two samples of 20 and 50 mg of ground plant tissue were collected from each plant for anthocyanin and chlorophyll/carotenoid extraction, respectively. Samples were stored in liquid  $\text{N}_2$  until use. Chlorophyll and carotenoid concentrations were quantified according to Lichtenthaler and Buschmann (2001, 2005) [27,28]. Anthocyanins were extracted using a method modified from Carvalho and Folta, 2014 [29], as previously described in Pocock (2016) [30]. All samples were measured spectrophotometrically in a V-570 UV/VIS/NIR spectrophotometer (Jasco Products Company, Oklahoma, OK, USA).

### 2.4. Fluorescence Undergraduate Sensing System: FUSSY

FUSSY consisted of an active LED light source and a photodiode-based detector which are described in detail below. The device had three basic components (described in detail below): (1) An LED excitation module which delivered an excitation pulse to the plant canopy, (2) A photodiode module which sensed and quantified chlorophyll fluorescence, and (3) A microcontroller which regulated the interval between the excitation pulses and moved the collected ChlF data to a cloud-based database. The excitation light source and the photodiode components were placed 50 cm from the crop canopy at 45° angles (Figure 1). The field of view of the photodiodes, and thus the area of the crop being sensed, was 12 cm in diameter. The device measured chlorophyll fluorescence at wavelengths of 680 nm and 740 nm using a six step process (described in Figure 2). The total cost of small volume production (five FUSSY units) was under \$400 USD per unit.

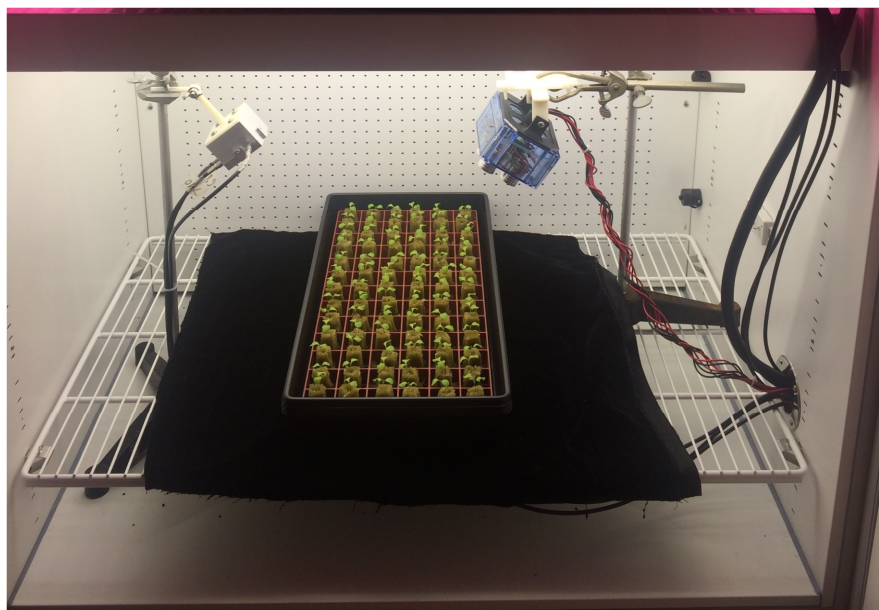


**Figure 1.** The excitation light source (right hand side) and the photodiode unit (left side) measuring ChlF of red lettuce in an controlled environment growth chamber. The individual components are described in more detail in the following sections.

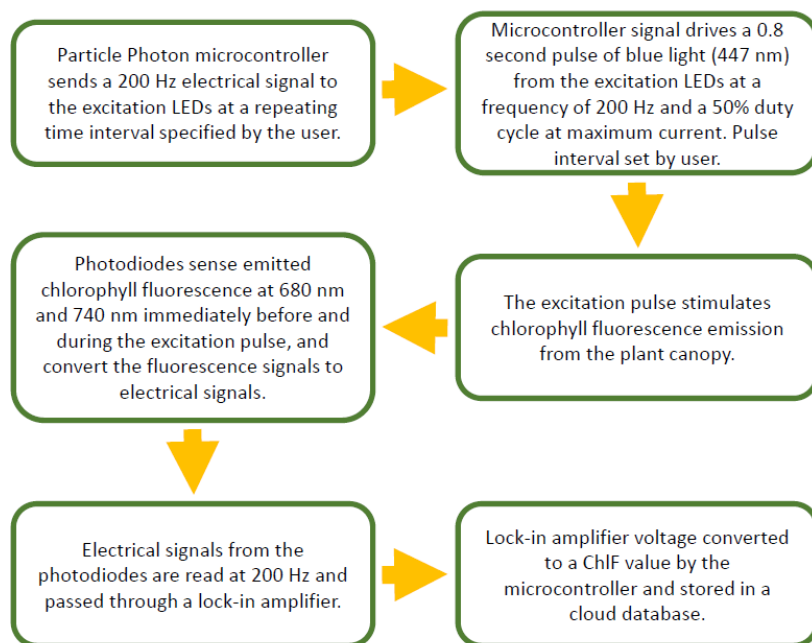


**Figure 2.** ChlF detection proceeded via six basic steps.

#### 2.4.1. Excitation LED Module

The excitation LED module consisted of four separate, custom made three chip royal blue (447 nm) LED units (LEDSupply, Inc., 3-up Royal Blue Star, Randolph, VT, USA), for a total of 12 LEDs per excitation module. Each LED used up to 3 watts of power, for a total of 36 watts. The photon flux density at crop level for the excitation pulses was  $2000 \mu\text{mol m}^{-2} \text{s}^{-1}$  PAR. The LEDs were driven by a custom 12 V driver board equipped with resistors and voltage regulators to prevent LED overload. The driver board was enclosed in a plastic casing to prevent moisture condensation on electrical components. The frequency was adjustable and, for these sets of experiments, the LED driver board was set to receive a 200 Hz electrical signal from the microcontroller via a 200 Hz coaxial signal cable.

#### 2.4.2. Photodiode Module

The photodiode module consisted of two photodiodes (Intor T-18, Intor, Inc., Socorro, NM, USA) that detect light of wavelengths of 680 nm and 740 nm, respectively. Each photodiode was equipped with a T-18 style, near collimated optical filter (Intor 680-10-50, 740-10-50, Intor Inc., Socorro, NM, USA) to limit incoming light to the desired wavelengths and field of view. This resulted in a field of view of 12 cm diameter at a distance of 50 cm from the plant canopy. Larger fields of view were possible at a greater distance from the canopy, but were limited based on the dimensions of the growth chamber. The photodiode was housed in a custom-built aluminum box milled from 6061 aluminum with wall thicknesses of  $\frac{1}{4}$  inch that shielded the detection electronics from ambient electrical interference.

#### 2.4.3. Microcontroller Boards

The system utilized a separate printed circuit board to process signals from each photodiode. The boards were powered by a 12 V power supply, with a 5 V output to the photodiodes and microcontroller. The board included a Particle Photon microcontroller (Analog Devices, 620, Analog Devices, Inc., Norwood, MA, USA) that controlled the excitation LED module. Signals from the Particle Photon microcontroller to the excitation LED module were carried by a coaxial cable attached to the board via an SMA (SubMiniature version A) connector. Pulses to the LED module were controlled by a custom-coded algorithm which runs on the Particle Photon microcontroller. All light at the desired wavelengths was absorbed by the photodiode and converted to an analog electrical signal that was passed to an AD620 chip for pre-processing amplification. The signal then passed through a

lock-in amplifier (AD630 chip, Analog Devices, Norwood, MA, USA) which removed any signal with a frequency other than 200 Hz. A low-pass filter and amplifier (Analog Devices, OP-07, Norwood, MA, USA) then removed all harmonic signals. This accounted for background RF interference and any trim issues in the amplifiers. The resulting data was stored in a database located in the cloud via a wireless network connection. ChlF measurements can be programmed to occur at any time interval greater than 0.8 s which is the time it takes to make a measurement. In this study measurements were taken every 15 min.

#### 2.4.4. Control System and Power Supply

The power supplies for the excitation LED module and the microcontroller printed circuit boards (PCBs) take standard 120 V, 60 Hz AC power as input and output 12 V power to the PCB boards and LED module. The LED driver board was connected to the microcontroller PCB via a BNC (Bayonet Neill–Concelman) cable. Power was delivered from the PCB power supply to both PCBs via a three-pin molex connector (Molex, 03-09-2032, Molex. Inc., Lisle, IL, USA). Power was delivered to the LED module via a larger twisted strand style cable connected to the power supply enclosure by a simple external connector.

#### 2.5. Data Processing, Statistical Analysis, and Modeling

ChlF was monitored at 15 min intervals over a 17 day growth period. To measure ChlF at each time point, groups of five measurements were taken both before and during the 0.8 s excitation pulse. The lowest and highest of the five measurements were dropped, and the remaining three measurements were averaged to arrive at the final value. ChlF was then calculated as the difference between averaged measurements before each pulse and those during each pulse. A black cloth control experiment demonstrated that ChlF signals emanating from plants were an order of magnitude larger than background noise (Figure A2). Models were constructed for each of FW, DW, and PA plotted as a function of ChlF<sub>740nm</sub> using polynomial regression as implemented by the ‘train’ function in the R package ‘caret’ [31,32]. Leave-one-out cross-validation (LOOCV) [33] was used as a resampling based performance measure for model validation and selection. Prediction intervals were estimated using the ‘predict’ function in the R package ‘stats’ [34]. The forward-stepwise selection procedure [33] was used to select the order of each polynomial model (i.e., a stepwise increase in the model order until the t-test for the highest order term is non-significant). Normalized root mean square error (NRMSE) was calculated as a basis for comparison of error between models using the following formula:

$$NRMSE = \frac{RMSE}{y_{\max} - y_{\min}} \quad (1)$$

where RMSE is the root mean square error for the regression model and  $y_{\max}$  and  $y_{\min}$  are the maximum and minimum values, respectively, of the dependent variable. Polynomial models constructed based on data from each of the two data processing strategies described above were used to predict DW and PA. Predicted values of DW and PA from each model were used to calculate the relative growth rate (RGR), leaf area ratio (LAR), and net assimilation rate (NAR) using the following equations:

$$RGR = \frac{\ln W_2 - \ln W_1}{t_2 - t_1} \quad (2)$$

$$LAR = \frac{1}{2} \left( \frac{A_1}{W_1} + \frac{A_2}{W_2} \right) \quad (3)$$

$$NAR = \left( \frac{W_2 - W_1}{t_2 - t_1} \right) \left( \frac{\ln A_2 - \ln A_1}{A_2 - A_1} \right) \quad (4)$$

where  $W_1$  and  $W_2$  are the dry weight for the first and second time point, respectively,  $A_1$  and  $A_2$  are the plant area for the first and second time point, respectively, and  $t_1$  and  $t_2$  are the days after

seeding for the first and second time points, respectively. Time points used in index calculations were chosen from the linear portion of plots of time versus natural log-transformed DW to ensure that they were within the exponential region of the growth curve. To avoid transformation bias, DW data for all replicates and time points were natural log transformed before calculating means and standard errors [11]. Indices were calculated using observed and predicted values from identical time points for each experimental replicate ( $n = 4$ ), and results were averaged to obtain final mean and standard error. RGR, LAR, and NAR calculated from predicted DW and PA were then compared to RGR, LAR, and NAR calculated from observed values to determine the accuracy of predicted values.

Pearson correlation coefficients and  $p$ -values were calculated for all combinations of measured variables (i.e., FW, DW, PA and ChlF; see Table 1) using the 'rcorr' function implemented in the R package Hmisc V4.1-0 [35]. Significance testing of differences between pigment levels at different time points was carried out using Student's  $t$ -test [36] as implemented in Microsoft Excel 2013 (Microsoft, Inc., Redmond, WA, USA).

Relative importance analysis of FW, DW, and PA as predictors of ChlF was carried out using the LMG measure [37,38] as implemented by the 'calc.relimp' function in the R package 'relaimpo' [39]. This method was selected for its ability to account for a high degree of multicollinearity between predictor variables (see [40] for review).

**Table 1.** Pearson correlation coefficients and  $p$ -values for correlations between measured quantities.

|      | Pearson Correlation Coefficient ( $r$ ) |       |       |       | Pearson Correlation Coefficient $p$ -Value |                         |                         |                         |
|------|---|-------|-------|-------|--|-------------------------|-------------------------|-------------------------|
|      | ChlF                                    | FW    | DW    | PA    | ChlF                                       | FW                      | DW                      | PA                      |
| ChlF | 1                                       | 0.921 | 0.934 | 0.947 | NA   | $5.697 \times 10^{-5}$  | $2.677 \times 10^{-5}$  | $1.024 \times 10^{-5}$  |
| FW   | 0.921                                   | 1     | 0.995 | 0.996 | $5.697 \times 10^{-5}$                     | NA                      | $1.943 \times 10^{-10}$ | $6.773 \times 10^{-11}$ |
| DW   | 0.934                                   | 0.995 | 1     | 0.998 | $2.677 \times 10^{-5}$                     | $1.943 \times 10^{-10}$ | NA                      | $5.366 \times 10^{-12}$ |
| PA   | 0.947                                   | 0.996 | 0.998 | 1     | $1.024 \times 10^{-5}$                     | $6.773 \times 10^{-11}$ | $5.366 \times 10^{-12}$ | NA                      |

NA = Not applicable, ChlF = Chlorophyll fluorescence at 740 nm, FW = Fresh weight, DW = Dry weight, PA = Plant area.

### 3. Results

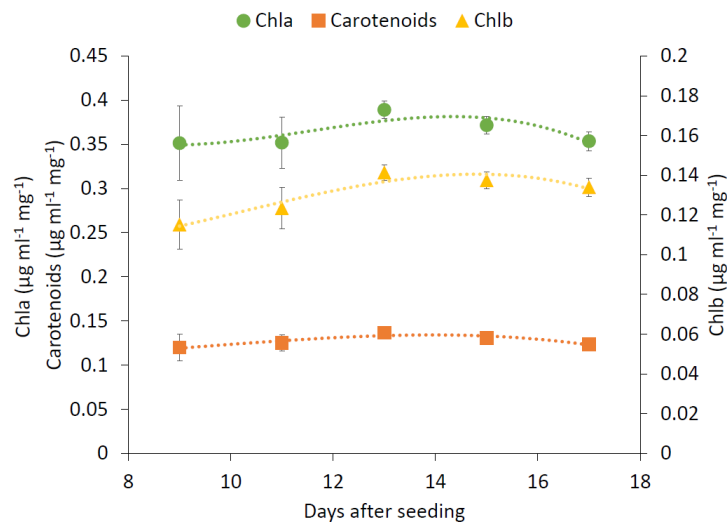
Manually- and remotely-sensed growth kinetics for red lettuce were performed and compared. ChlF measured both at 680 nm and 740 nm were collected and although they followed similar trends, ChlF<sub>740nm</sub> was used for the following analyses as it was a more robust and stable signal during the experimental periods. This was not due to the potential additive effects of reflectance since 740 nm was absent from the ambient light source. A suggested explanation could be the differences in the design of the photodiodes or their respective optical filters.

#### 3.1. Correlations between ChlF and Other Measured Quantities

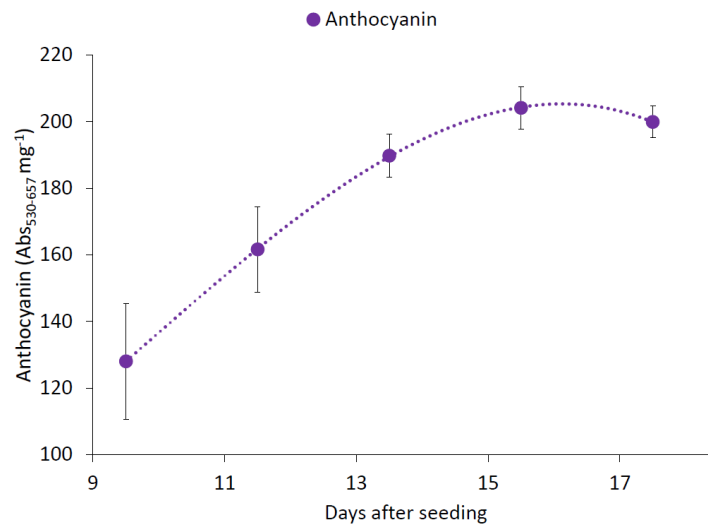
Pearson correlation coefficients ( $r$ ) and  $p$ -values were calculated to determine the strength and direction of the relationship between all combinations of measured variables (Table 1). ChlF showed a strong positive correlation with all measured quantities.

#### 3.2. Leaf Chlorophyll, Carotenoid, and Anthocyanin Concentrations

Chlorophyll and carotenoid concentrations were assayed at five time points between nine days after seeding (DAS) and 17 DAS (Figure 3). No significant change in mean chlorophyll a (Chla) or carotenoid content was observed in harvested plants during this period. Conversely, mean chlorophyll b (Chlb) concentrations significantly increased from 9 DAS to 13 DAS ( $p < 0.05$ ), after which no significant change was observed. Anthocyanin concentrations were measured at the same time intervals as chlorophylls and carotenoids and significantly increased 1.6-fold from 9 DAS to 15 DAS ( $p < 0.001$ ) after which they remained stable.



(A)



(B)

**Figure 3.** Chlorophyll (A) and carotenoid (B) concentrations in red lettuce ‘Rouxai’ plants during 17-day growth experiments. Values represent means from four experimental replicates ( $n = 12$ ). Error bars show standard errors of the mean (SEM). Error bars smaller than symbols are not visible.

### 3.3. Polynomial Regression Modeling

The relationship between mean ChlF and mean fresh weight (FW), dry weight (DW), and plant area (PA) was quantified using polynomial regression (Figure 4). The root mean square error (RMSE) of all final models normalized to the observed range of values for the modeled variable was less than 5%, with the models for PA and DW as a function of ChlF having the lowest (3.2%) and highest (4.1%) NRMSE, respectively. The trend was the same for the average NRMSE for models built from LOOCV training sets, which was highest for DW (6.2%) and lowest for PA (3.7%).

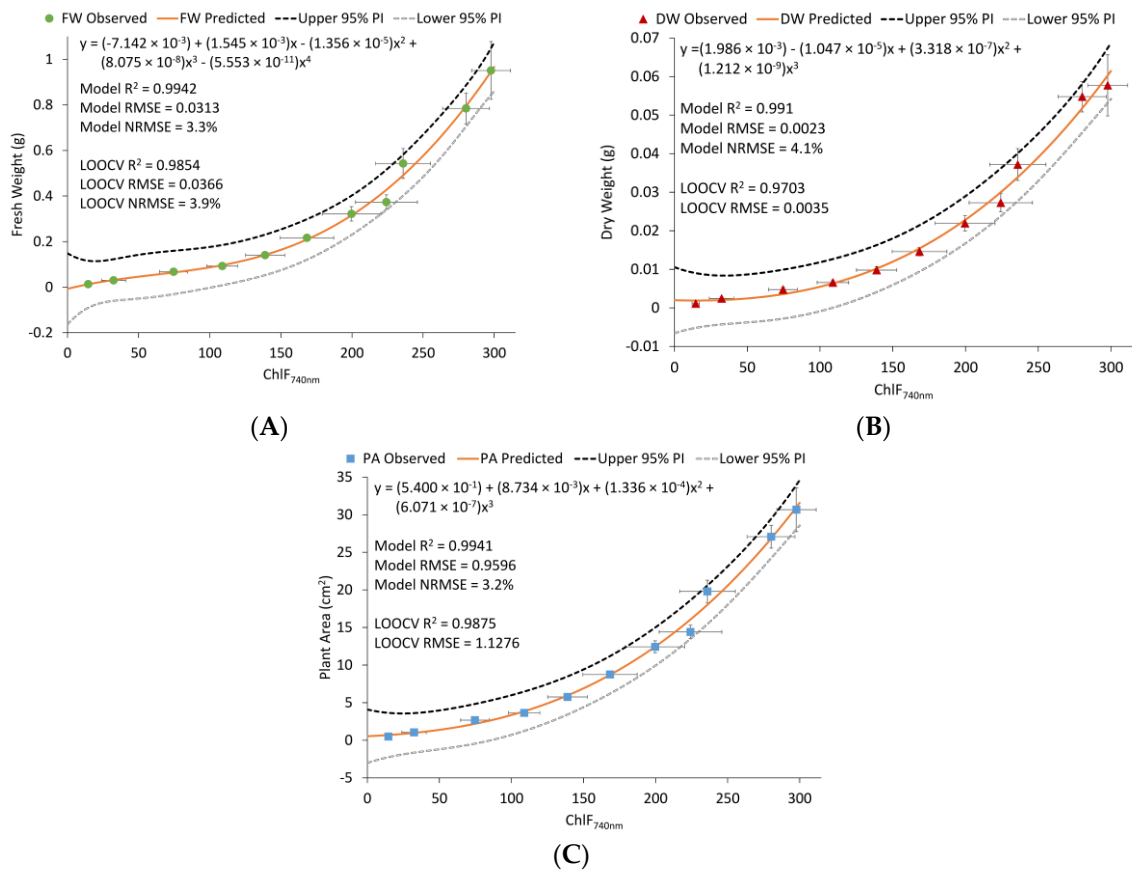


**Figure 4.** Final polynomial regression results for fresh weight (A), dry weight (B), and plant area (C), plotted as a function of chlorophyll fluorescence (ChlF<sub>740nm</sub>). Values represent means across four experimental replicates (*n* = 12). Dashed lines indicate 95% prediction intervals (PI). Error bars show standard errors of the mean (SEM).

### 3.4. Analysis of Variance of ChlF

Multiple linear regression modeling of ChlF<sub>740nm</sub> as a function of FW, DW and PA was followed by relative importance analysis to investigate sources of variation in mean ChlF (Figure 5). Plant area (PA) explained 4.7% and 5.3% more of the variance in ChlF than FW and DW, respectively.

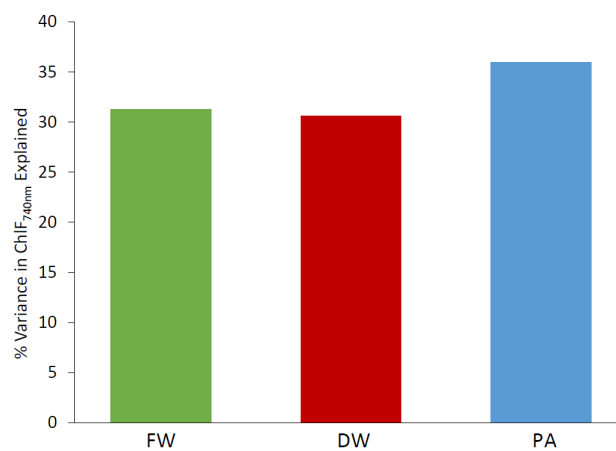


**Figure 5.** Percent variance in ChlF<sub>740nm</sub> explained by fresh weight (FW), dry weight (DW) and plant area (PA) of experimental plants as determined by multiple linear regression, followed by relative importance analysis.

### 3.5. Comparison of Observed and Predicted Growth Indices

Commonly-used growth indices were calculated from mean observed and predicted values of FW, DW and PA to evaluate model performance and demonstrate that ChlF measured by FUSSY could serve as an adequate proxy for these physical growth parameters (Figure 6). No significant differences were observed between the average values of growth indices calculated from observed values, as compared to those calculated from values predicted by the FUSSY approach.

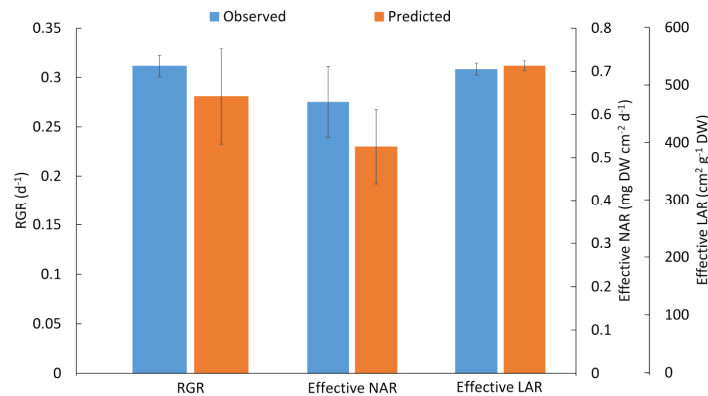


**Figure 6.** Relative growth rate (RGR), net assimilation rate (NAR), and leaf area ratio (LAR) calculated from observed and predicted dry weight and plant area values. Values are means of indices calculated with data from each experimental replicate ( $n = 4$ ). Error bars show standard errors of the mean (SEM).

## 4. Discussion

To the best of our knowledge, the ChlF sensing device described in this paper is the first example of an inexpensive, remote ChlF detection system purpose-built for the real-time tracking of physical plant growth parameters in a controlled environment. Some previous ChlF detection systems developed for CEA have focused on utilizing ChlF as a signal of photochemical efficiency, rather than as a proxy for growth, with the end goal of optimizing plant growth rates indirectly through the optimization of photosynthetic performance [22]. Others have combined reflectance and ChlF measurements at multiple wavelengths to estimate plant biomass using relatively complex and costly spectral methods [21]. In contrast, we have demonstrated that far red ChlF emission at 740 nm (ChlF<sub>740nm</sub>) measured in the light-adapted state is strongly correlated with observed changes in FW, DW and PA of experimental plants (Table 1). It can, therefore, serve as a simple, remotely-measured proxy for plant growth without the need for computationally expensive data processing or standard destructive methods.

The strong positive correlation observed between ChlF<sub>740nm</sub> and PA, FW, and DW has two possible explanations. First, because fluorescence at 740 nm is emitted by chlorophyll *a* (Chl*a*) molecules [41,42], the observed increase in ChlF<sub>740nm</sub> could potentially be the result of increasing concentrations of Chl*a*, relative to total plant mass. However, Chl*a* concentrations in our experimental plants did not change significantly over the course of the experiment (Figure 3A), indicating that Chl*a* concentrations were not responsible for the observed increases in ChlF<sub>740nm</sub>. Red lettuce also contains the red pigment anthocyanin that acts as a sunscreen and functions to attenuate light from reaching the photosynthetic apparatus where Chl*a* molecules are located. This attenuating effect could also reduce the level of light from ChlF<sub>740nm</sub> being emitted from the leaf. However, while anthocyanin concentrations did increase during growth (Figure 3B), the strong correlation between the ChlF<sub>740nm</sub> signal and PA, FW, and DW indicates that the presence of anthocyanin did not attenuate the ChlF signal significantly during growth. Together with the lack of any variation in Chl*a* content over the course of the experiment, this suggests that physiological changes, rather than biochemical changes, in the plant are likely driving the observed changes in ChlF<sub>740nm</sub>. Second, given that Chl*a* resides in the chloroplasts within plant cells, it is likely that the majority of the variation in ChlF<sub>740nm</sub> can be explained by changes in the overall

photosynthetic surface area exposed to the excitation pulse emitted by the detector. Consistent with this suggestion, relative weights analysis of a multiple linear regression model of  $\text{ChlF}_{740\text{nm}}$  as a function of FW, DW, and PA indicated that PA explained roughly 5% more of the total explained variance in  $\text{ChlF}_{740\text{nm}}$  than FW or DW (Figure 5). This result could also explain why  $\text{ChlF}_{740\text{nm}}$  plotted as a function of time approached an upper asymptote in three of four experimental replicates (Figure A1). Once PA became large enough to fill the area of effect of the excitation light and photodiode module, the photosynthetic surface area (and, as a result,  $\text{ChlF}_{740\text{nm}}$ ) would no longer increase. Due to space constraints in the growth chambers, the plants were grown until the baby leafy green stage (17 days). The growth curves indicated that the lettuce crop was still in exponential growth and had not reached the stationary phase when full heads would be harvested (Figure A1). FUSSY needs to be tested and validated in sunlight over a larger area where plant growth is not limited by space. Initial testing in a greenhouse did reveal that the optical system was operational in full sun without saturation issues. Growth rate testing is currently under way as part of the Greenhouse Lighting and Systems Engineering Consortium (GLASE) at Cornell University, Ithaca, NY. There does not appear to be a reason for FUSSY not to work as a proxy for growth during the entire red lettuce life cycle as long as the crop is not space constrained.

Plotting FW, DW, and PA as a function of  $\text{ChlF}_{740\text{nm}}$  revealed a nonlinear relationship between plant growth and fluorescence emission that was best described by polynomial regression modeling (Figure 4). Normalized root mean square error (NRMSE) of models varied from 3.3% to 4.1% of the predicted variable's range, indicating both a reasonably small difference between predicted and observed values for each model, and a consistent predictive accuracy across models. These NRMSE values also compare favorably to those of previous models of plant growth as a function of ChlF. For example, linear models based on the natural log (ln) of basil plant dry weight as a function of the ln of the ratio of red to far red ChlF resulted in NRMSE values of between 5.1% and 7.4% [21], as compared to an NRMSE of 4.1% for the polynomial models of dry weight as a function of  $\text{ChlF}_{740\text{nm}}$  in this study. In addition, ln-transformation of DW introduces an additional layer of complexity to the interpretation of model predictions, and may result in statistically-biased predictions [43]. By contrast, our measurement of a single ChlF wavelength and polynomial modeling from untransformed data both avoids these potential statistical pitfalls and makes the prediction of growth parameters from ChlF data more practical for the grower.

Values for RGR, NAR, and LAR calculated from predicted mean values for DW and PA were within 10% of those calculated from observed mean values of DW and PA, though the difference was not statistically significant (Figure 6). Examples of studies utilizing RGR, NAR, and LAR from the literature indicate that 10% variation is well within the typical error range for these indices. For example, Shipley (2006) [44] calculated a within-study variance of 14% of the mean in both RGR and NAR from 83 different experiments published in 37 different studies involving both woody and herbaceous species. These results demonstrate that  $\text{ChlF}_{740\text{nm}}$  measured by our device can serve as a reliable proxy for plant growth that has numerous potential applications in physiological and ecophysiological research, as well as commercial CEA settings. One such application is made possible by recent advances in light emitting diode (LED) systems which have provided an unprecedented level of lighting control through feedback and dynamic algorithms [22,45,46]. Such control offers growers the opportunity to maximize light use efficiency [47] and optimize morphological and physiological characteristics of their crop through manipulation of spectral composition [30,48,49]. However, the full realization of the enormous cost-saving potential that LED lighting provides to the CEA industry will require new and innovative light control systems that encapsulate real-time physiological data in their decision-making algorithms. Ideally, such control systems would be fully automated to minimize measurement error and labor costs. The results presented in this study demonstrate that our ChlF detector, FUSSY, could function as an integral piece of such an automated light control system by providing direct, real-time tracking of multiple plant growth parameters without the need for expensive equipment, computationally expensive calculations, or labor-intensive data collection.

## 5. Conclusions

Control systems in CEA facilities are built on sophisticated models that are based solely on environmental inputs. The overall goal of this work was to develop a small, inexpensive sensor that could be integrated into CEA lighting control systems. Adding biological inputs to CEA control algorithms has the potential to improve crop management and resource use efficiency. While FUSSY was able to accurately predict red lettuce growth rates, more testing needs to be done. Further research includes monitoring the growth of crops with different leaf and plant architectures (i.e., waxy cuticle, hairy leaves, taller plants), testing the performance of FUSSY in additional growth settings (e.g., greenhouses or vertical farms), and documenting the system's ability to detect physiological changes in plants related to environmental stressors (e.g., drought, nutrient limitation, temperature stress, and disease, among others). Validation of FUSSY's performance under different light sources should also be carried out to ensure stable ChlF readings under different spectra, photon flux densities and frequencies.

**Author Contributions:** T.P. conceived and designed the experiments. M.R.U. performed the experiments and analyzed the data. T.P. and M.R.U. wrote the paper. T.P. designed the sensing system and managed undergraduate development and assembly teams. T.P. contributed reagents and materials. Invaluable editorial feedback was provided by A.J. Both, Director, Center for Controlled Environment Agriculture, Rutgers University, NJ.

**Funding:** This work was supported primarily by the New York State research and Development Authority (NYSERDA) contract 107303 and in part by the Engineering Research Centers Program (ERC) of the National Science Foundation under NSF Cooperative Agreement No. EEC-0812056 and in part by New York State under NYSTAR contract C090145. Funds are available for covering the costs to publish in open access.

**Acknowledgments:** The authors would like to acknowledge Robert Karlicek and the engineering support staff at RPI for their guidance. Lastly, this work would not have been possible without the creativity and dedication of engineering undergraduate students namely, Andrew Turk, Shenwei Li, Yunqi Liu, Leen Al Madani, Will Johnson, Sean O'Connor, Regan Callan, Adam Circle, Zhiheng Zhang, Mandy Liu, and Yuhan Shi.

**Conflicts of Interest:** The authors declare no conflicts of interest.

## Appendix A

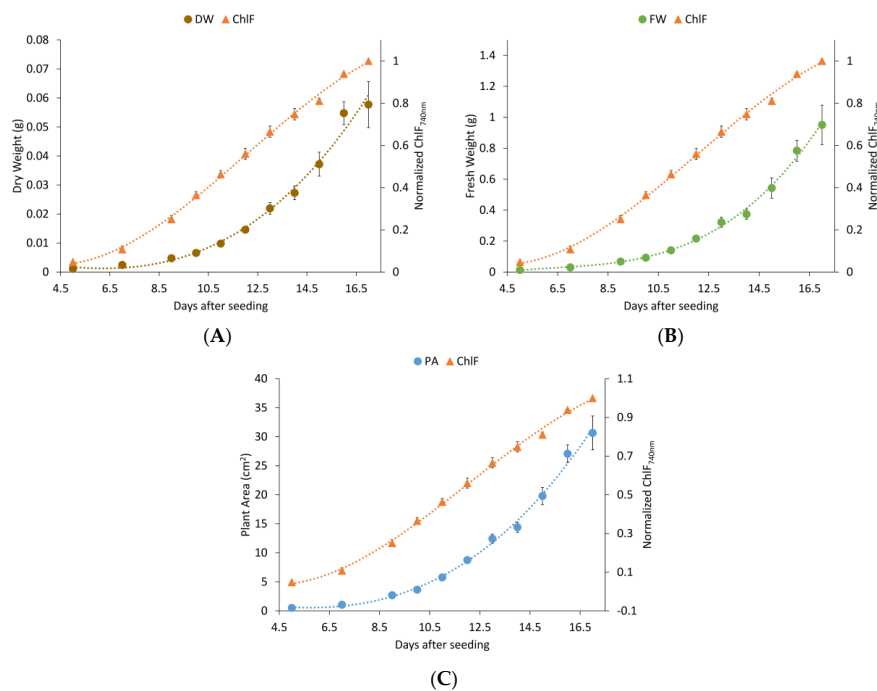


**Figure A1.** Dry weight (DW) (A), fresh weight (FW) (B), plant area (PA) (C) and relative chlorophyll fluorescence values (ChlF) as a function of days after seeding. Values are means of observed values from four experimental replicates ( $n = 12$ ). Error bars show standard error of the means (SEM).

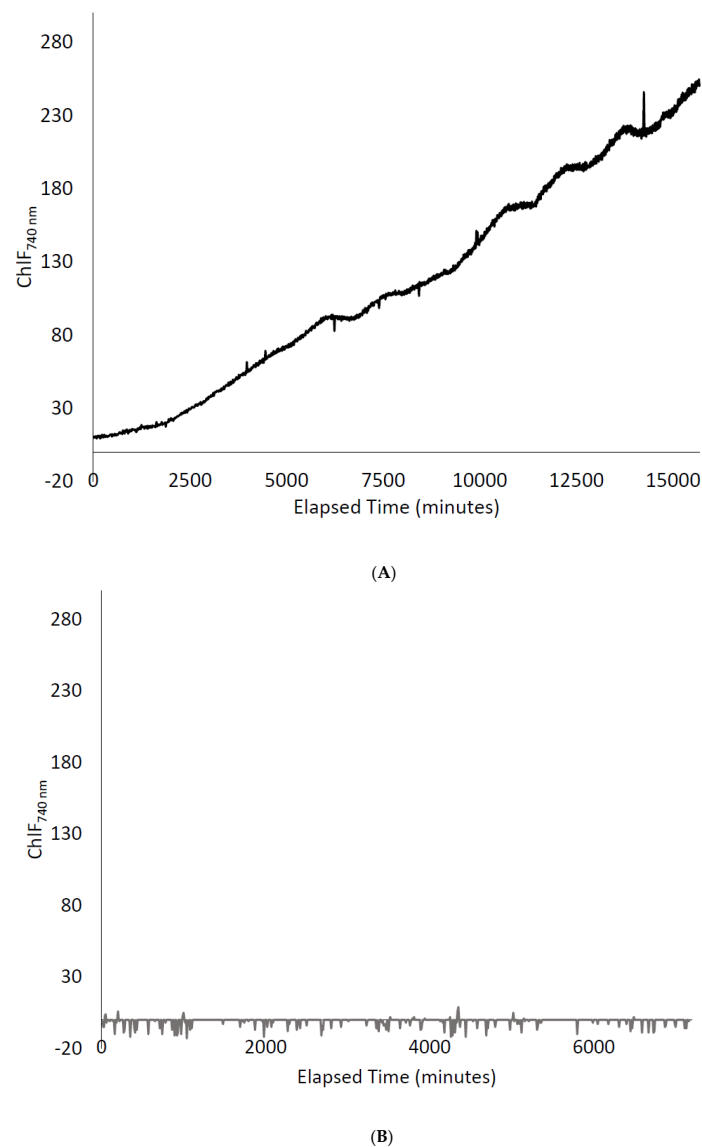


**Figure A2.** Chlorophyll fluorescence signal from growing lettuce plants (A) and from a black cloth control used to determine measurement noise (B). Both datasets are plotted on the same vertical scale to facilitate comparison of signal magnitude to noise magnitude.

## References

1. Beddington, J.R.; Asaduzzaman, M.; Clark, M.E.; Fernández Bremauntz, A.; Guillou, M.D.; Howlett, D.J.B.; Jahn, M.M.; Lin, E.; Mamo, T.; Negra, C.; et al. Agriculture: What next for agriculture after Durban? *Science* **2012**, *335*, 289–290. [[CrossRef](#)] [[PubMed](#)]
2. Supit, I.; van Diepen, C.A.; De Wit, A.J.W.; Wolf, J.; Kabat, P.; Baruth, B.; Ludwig, F. Assessing climate change effects on European crop yields using the Crop Growth Monitoring System and a weather generator. *Agric. For. Meteorol.* **2012**, *164*, 96–111. [[CrossRef](#)]
3. Ehret, D.; Lau, A.; Bittman, S.; Lin, W.; Shelford, T.; Ehret, D.; Lau, A.; Bittman, S.; Lin, W.; Shelford, T. Automated monitoring of greenhouse crops. *Agronomie* **2001**, *21*, 403–414. [[CrossRef](#)]
4. Harbick, K.; Albright, L.D. Comparison of energy consumption: Greenhouses and plant factories. *Acta Hortic.* **2016**, *1134*, 285–292. [[CrossRef](#)]
5. Albright, L.D.; Both, A.-J.; Chiu, A.J. Controlling greenhouse light to a consistent daily integral. *Trans. ASAE* **2000**, *43*, 421–431. [[CrossRef](#)]

6. Harbick, K.; Albright, L.D.; Mattson, N.S. Electrical savings comparison of supplemental lighting control systems in greenhouse environments. In Proceedings of the 2016 ASABE Annual International Meeting, Orlando, FL, USA, 17–20 July 2016; American Society of Agricultural and Biological Engineers: St. Joseph, MI, USA, 2016; p. 1.
7. Pocock, T. Light-emitting diodes and the modulation of specialty crops: Light sensing and signaling networks in plants. *Hortic. Sci.* **2015**, *50*, 1281–1284.
8. Hunt, R. *Basic Growth Analysis. Plant Growth Analysis for Beginners*; Unwin Hyman: London, UK, 1990.
9. Gillner, S.; Rüger, N.; Roloff, A.; Berger, U. Low relative growth rates predict future mortality of common beech (*Fagus sylvatica* L.). *For. Ecol. Manag.* **2013**, *302*, 372–378. [[CrossRef](#)]
10. Qiu, R.; Wei, S.; Zhang, M.; Li, H.; Sun, H.; Liu, G.; Li, M. Sensors for measuring plant phenotyping: A review. *Int. J. Agric. Biol. Eng.* **2018**, *11*, 1–17. [[CrossRef](#)]
11. Hoffmann, W.A.; Poorter, H. Avoiding bias in calculations of relative growth rate. *Ann. Bot.* **2002**, *90*, 37–42. [[CrossRef](#)] [[PubMed](#)]
12. Tessmer, O.L.; Jiao, Y.; Cruz, J.A.; Kramer, D.M.; Chen, J. Functional approach to high-throughput plant growth analysis. *BMC Syst. Biol.* **2013**, *7*, S17. [[CrossRef](#)] [[PubMed](#)]
13. Misra, A.N.; Misra, M.; Singh, R. Chlorophyll fluorescence in plant biology. In *Biophysics*; Misra, A.N., Ed.; InTech Open: London, UK, 2012; ISBN 9789537619992.
14. Kalaji, H.M.; Schansker, G.; Brestic, M.; Bussotti, F.; Calatayud, A.; Ferroni, L.; Goltsev, V.; Guidi, L.; Jajoo, A.; Li, P.; et al. Frequently asked questions about chlorophyll fluorescence, the sequel. *Photosynth. Res.* **2017**, *132*, 13–66. [[CrossRef](#)] [[PubMed](#)]
15. Strasser, R.J.; Srivastava, A.; Tsimilli-Michael, M. The fluorescence transient as a tool to characterize and screen photosynthetic samples. *Probing Photosynth. Mech. Regul. Adapt.* **2000**, *25*, 443–480.
16. Maxwell, K.; Johnson, G.N. Chlorophyll fluorescence—A practical guide. *J. Exp. Bot.* **2000**, *51*, 659–668. [[CrossRef](#)] [[PubMed](#)]
17. Fernandez-Jaramillo, A.A.; Duarte-Galvan, C.; Contreras-Medina, L.M.; Torres-Pacheco, I.; Romero-Troncoso, R.D.; Guevara-Gonzalez, R.G.; Millan-Almaraz, J.R. Instrumentation in developing chlorophyll fluorescence biosensing: A review. *Sensors* **2012**, *12*, 11853–11869. [[CrossRef](#)] [[PubMed](#)]
18. Govindjee, G. Chlorophyll a fluorescence: A bit of basics and history. In *Chlorophyll A Fluorescence A Signature of Photosynthesis*; Springer: New York, NY, USA, 2004; pp. 1–42.
19. Magney, T.S.; Frankenberg, C.; Fisher, J.B.; Sun, Y.; North, G.B.; Davis, T.S.; Kornfeld, A.; Siebke, K. Connecting active to passive fluorescence with photosynthesis: A method for evaluating remote sensing measurements of Chl fluorescence. *New Phytol.* **2017**, *215*, 1594–1608. [[CrossRef](#)] [[PubMed](#)]
20. Ahlman, L.; Bänkestad, D.; Wik, T. Using chlorophyll a fluorescence gains to optimize LED light spectrum for short term photosynthesis. *Comput. Electron. Agric.* **2017**, *142*, 224–234. [[CrossRef](#)]
21. Bänkestad, D.; Wik, T. Growth tracking of basil by proximal remote sensing of chlorophyll fluorescence in growth chamber and greenhouse environments. *Comput. Electron. Agric.* **2016**, *128*, 77–86. [[CrossRef](#)]
22. Van Iersel, M.W.; Weaver, G.; Martin, M.T.; Ferrarezi, R.S.; Mattos, E.; Haidekker, M. A chlorophyll fluorescence-based biofeedback system to control photosynthetic lighting in controlled environment agriculture. *J. Am. Soc. Hortic. Sci.* **2016**, *141*, 169–176.
23. Kliewer, W.M.; Dokoozlian, N.K. Leaf area/crop weight ratios of grapevines: Influence on fruit composition and wine quality. *Am. J. Enol. Vitic.* **2005**, *56*, 170–181.
24. Machado, S.; Bynum, E.D.; Archer, T.L.; Lascano, R.J.; Wilson, L.T.; Bordovsky, J.; Segarra, E.; Bronson, K.; Nesmith, D.M.; Xu, W. Spatial and temporal variability of corn growth and grain yield: Implications for site-specific farming. *Crop Sci.* **2002**, *42*, 1564–1576. [[CrossRef](#)]
25. Hoagland, D.R.; Arnon, D.I. The water-culture method for growing plants without soil. *Circ. Calif. Agric. Exp. Stn.* **1950**, *347*, 32.
26. Easlon, H.M.; Bloom, A.J. Easy leaf area: Automated digital image analysis for rapid and accurate measurement of leaf area. *Appl. Plant Sci.* **2014**, *2*, 1400033. [[CrossRef](#)] [[PubMed](#)]
27. Lichtenthaler, H.K.; Buschmann, C. Extraction of photosynthetic tissues: Chlorophylls and carotenoids. *Curr. Protoc. Food Anal. Chem.* **2001**. [[CrossRef](#)]
28. Lichtenthaler, H.K.; Buschmann, C. Chlorophylls and carotenoids: Measurement and characterization by uv-vis spectroscopy. *Handb. Food Anal. Chem.* **2005**, *2*, 171–178. [[CrossRef](#)]

29. Carvalho, S.D.; Folta, K.M. Sequential light programs shape kale (*Brassica napus*) sprout appearance and alter metabolic and nutrient content. *Hortic. Res.* **2014**, *1*, 1–13. [[CrossRef](#)] [[PubMed](#)]
30. Pocock, T. Advanced lighting technology in controlled environment agriculture. *Light. Res. Technol.* **2016**, *48*, 83–94. [[CrossRef](#)]
31. Kuhn, A.M.; Wing, J.; Weston, S.; Williams, A. The Caret Package. Available online: <http://topepo.github.io/caret/index.html> (accessed on 26 May 2018).
32. Kuhn, M. Caret: Classification and Regression Training; Version 6.0–7.6, Version R Package. Available online: <http://adsabs.harvard.edu/abs/2015ascl.soft05003K> (accessed on 3 May 2015).
33. Hastie, T.; Tibshirani, R.; Friedman, J. The elements of statistical learning. *Math. Intell.* **2001**, *27*, 83–85. [[CrossRef](#)]
34. Team, R.C. *R: A Language and Environment for Statistical Computing*; R Foundation for Statistical Computing: Vienna, Austria, 2017.
35. Harrell, F.E., Jr. Hmisc: Harrell Miscellaneous. Available online: <http://biostat.mc.vanderbilt.edu/Hmisc>, <https://github.com/harrelfe/Hmisc> (accessed on 3 January 2018).
36. Haynes, W. Student's *t*-Test. In *Encyclopedia of Systems Biology*; Dubitzky, W., Wolkenhauer, O., Cho, K.-H., Yokota, H., Eds.; Springer: New York, NY, USA, 2013; pp. 2023–2025; ISBN 978-1-4419-9863-7.
37. Lindeman, R.H.; Merenda, P.F.; Gold, R.Z. *Introduction to Bivariate and Multivariate Analysis*; Foresman and Co.: London, UK, 1980.
38. Kruskal, W. *Relative Importance by Averaging Over Orderings*; Taylor & Francis, Ltd.: Abingdon, UK, 2017; Volume 41, pp. 6–10.
39. Grömping, U. R package relaimpo: Relative importance for linear regression. *J. Stat. Softw.* **2006**, *17*, 139–147. [[CrossRef](#)]
40. Bi, J. A review of statistical methods for determination of relative importance of correlated predictors and identification of drivers of consumer liking. *J. Sens. Stud.* **2012**, *27*, 87–101. [[CrossRef](#)]
41. Krause, G.H.; Weis, E. Chlorophyll fluorescence and photosynthesis: The basics. *Annu. Rev. Plant Physiol. Plant Mol. Biol.* **1991**, *42*, 313–349. [[CrossRef](#)]
42. Pedrós, R.; Moya, I.; Goulas, Y.; Jacquemoud, S. Chlorophyll fluorescence emission spectrum inside a leaf. *Photochem. Photobiol. Sci.* **2008**, *7*, 498. [[CrossRef](#)] [[PubMed](#)]
43. Newman, M.C. Regression analysis of log-transformed data—statistical bias and its correction (short communication). *Environ. Toxicol. Chem.* **1993**, *12*, 1129–1133. [[CrossRef](#)]
44. Shipley, B. Net assimilation rate, specific leaf area and leaf mass ratio: Which is most closely correlated with relative growth rate? A meta-analysis. *Funct. Ecol.* **2006**, *20*, 565–574. [[CrossRef](#)]
45. Kozai, T.; Niu, G.; Takagaki, M. *Plant Factory: An Indoor Vertical Farming System for Efficient Quality Food Production*; Elsevier: London, UK, 2015.
46. Pocock, T. Influence of light-emitting diodes (LEDs) on light sensing and signaling networks in plants. In *Light Emitting Diodes for Agriculture*; Springer: Berlin, Germany, 2017; pp. 37–58.
47. Pinho, P.; Hytönen, T.; Rantanen, M.; Elomaa, P.; Halonen, L. Dynamic control of supplemental lighting intensity in a greenhouse environment. *Light. Res. Technol.* **2013**, *45*, 295–304. [[CrossRef](#)]
48. Fukuda, N. Advanced Light Control Technologies in Protected Horticulture: A review of morphological and physiological responses in plants to light quality and its application. *J. Dev. Sustain. Agric.* **2013**, *40*, 32–40. [[CrossRef](#)]
49. Ouzounis, T.; Rosenqvist, E.; Ottosen, C.O. Spectral effects of artificial light on plant physiology and secondary metabolism: A review. *Hortic. Sci.* **2015**, *50*, 1128–1135.

